Optically stimulated luminescence (OSL) dating of coversand deposits from Flixborough, Lincolnshire

Jean-Luc Schwenninger

Summary: A series of samples was collected from two trenches near Flixborough in Lincolnshire for optically stimulated luminescence dating (OSL). The dates were obtained from sand-sized quartz grains and palaeodose determinations were made using a single aliquot regenerative-dose (SAR) protocol. The environmental dose rate for each sample was calculated using the results obtained by neutron activation analysis (NAA) and *in situ* gamma-ray spectroscopy measurements. The concentrations of radioactive elements were above detection limits and the samples and their luminescence characteristics were close to optimal for obtaining reliable luminescence age estimates.

Keywords:
Optically stimulated luminescence
Geochronology

Author's address: *Research Laboratory for Archaeology and the History of Art, University of Oxford, 6 Keble Road, Oxford OX1 3QJ*

Introduction

Late Pleistocene windblown sand deposits cover large areas of lowland in north-central Europe, and probably once extended over much of eastern England. A discontinuous area of *c* 400 km^2 survives west of the Lincolnshire Wolds, between Gainsborough and the River Humber. Periglacial coversand deposits in this area are often up to several metres thick and a well dated regional stratigraphy based on luminescence dates has already been established by Bateman (1995; 1998) and Bateman et *al* (2000). Although primarily deposited during the Younger Dryas episode (12,500–11,400 cal BP) (*ibid*), the Lincolnshire coversands have evidently been reworked more recently, as stray and *in situ* archaeological finds of all periods from the Mesolithic onwards have been found during sand extraction. The aim of the project's scientific dating programme was to determine whether it was possible to use optically stimulated luminescence (OSL) to date episodes of sand re-deposition during the Holocene and thus, archaeological resources preserved within the sandsheets. The excavation of an Iron Age site near Flixborough (Fig 1) provided an opportunity to establish a chronological framework based on OSL dates in a type of sedimentary environment often unsuitable to the preservation of organic material and where the application of radiocarbon dating is very limited.

The site is located within an area known as the Willow Holt Quarry Extension (SMR 19690; NGR SE 8715 1460; 53.37.14N, 0.40.56W), where several archaeological sites were identified during an earlier evaluation (SMR numbers 19690-91; 19693-95). Site 19690, which first appeared as a shallow anomaly during the geophysical survey of the quarry extension, was investigated by test excavation, exposing an area of burnt clay and a large stone slab, 0.1m below the modern surface. Three successive occupation layers, separated by windblown sand deposits, were noted during sand extraction, and animal bones, Iron Age pottery, and a fragment of a clay metalworking mould were recovered. The site was excavated by the Lincolnshire coversands project in 2003 and was coordinated by J McIlwaine at the Department of Archaeological Sciences, University of Bradford.

A series of 13 samples was collected on the 19th of June 2003 by Dr J-L Schwenninger from two trenches (trench 1 and trench 3). *In situ* gamma dose rate measurements were made with an EG&G Ortec MicroNomad NaI gamma-ray spectrometer. Further details regarding individual samples are presented in Table 1 and their precise location within individual trenches is shown in Figures 2 and 3.

Field code	Lab. code	Trench	Depth (cm)	Comments on sedimentary unit
FLX03-01	X1684	Trench 3	375	Orange silty sand
FLX03-02	X1685	Trench 3	335	Yellow sand
FLX03-03	X1686	Trench 3	250	Yellow sand
FLX03-04	X1687	Trench 3	200	Yellowish brown sand
FLX03-05	X1688	Trench 1	65	Yellow sand
FLX03-06	X1689	Trench 1	100	Yellow sand
FLX03-07	X1690	Trench 1	65	Recently disturbed sand
FLX03-08	X1691	Trench 1	145	Black sand with charred plant remains
FLX03-09	X1692	Trench 1	160	Yellow white sand
FLX03-10	X1693	Trench 1	210	Grey sand – Buried soil A horizon?
FLX03-11	X1694	Trench 1	250	Yellow sand
FLX03-12	X1695	Trench 1	300	White sand
FLX03-13	X1696	Trench 1	150	Black sand; replicate sample of FLX03-08

Table 1 Sample details. The sample depth refers to the depth below ground surface

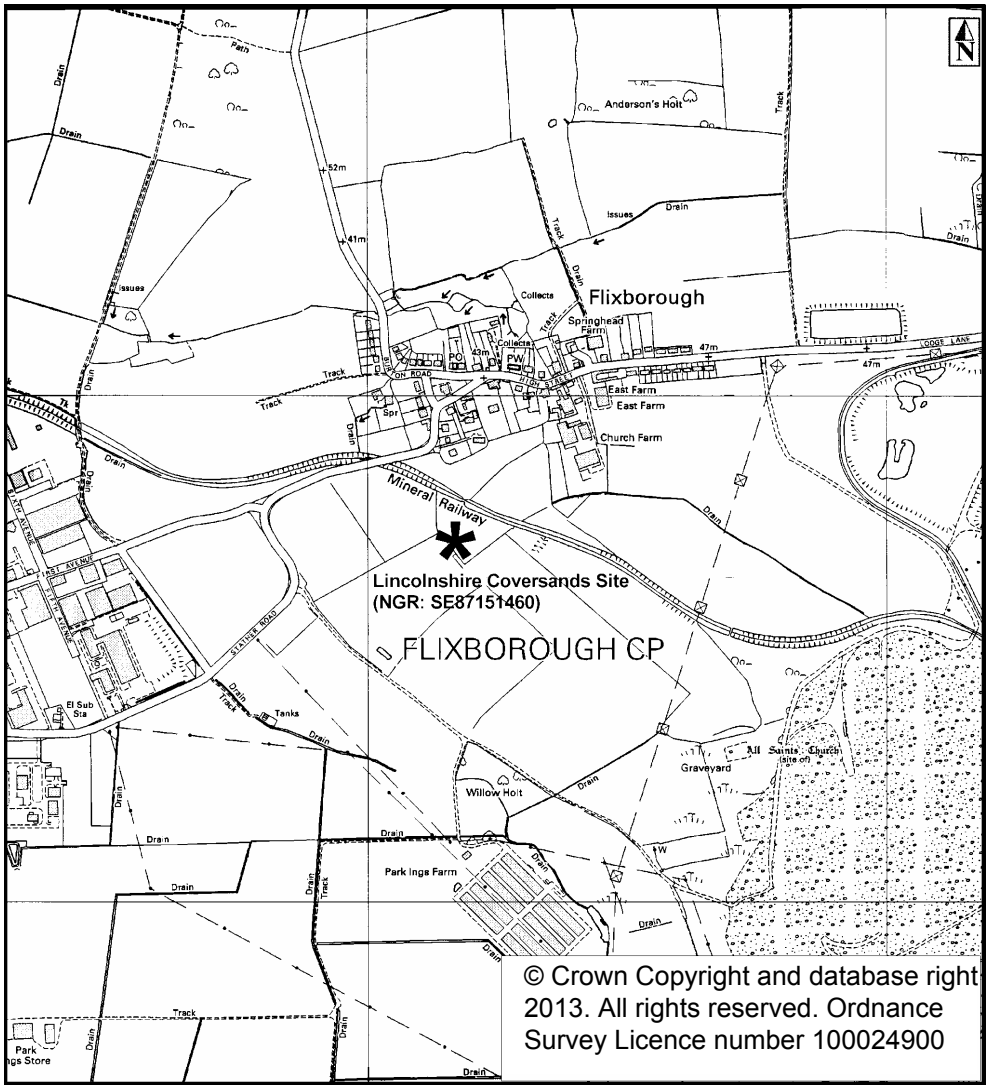

Figure 1 Map featuring the location of the archaeological excavation near Flixborough in North Lincolnshire

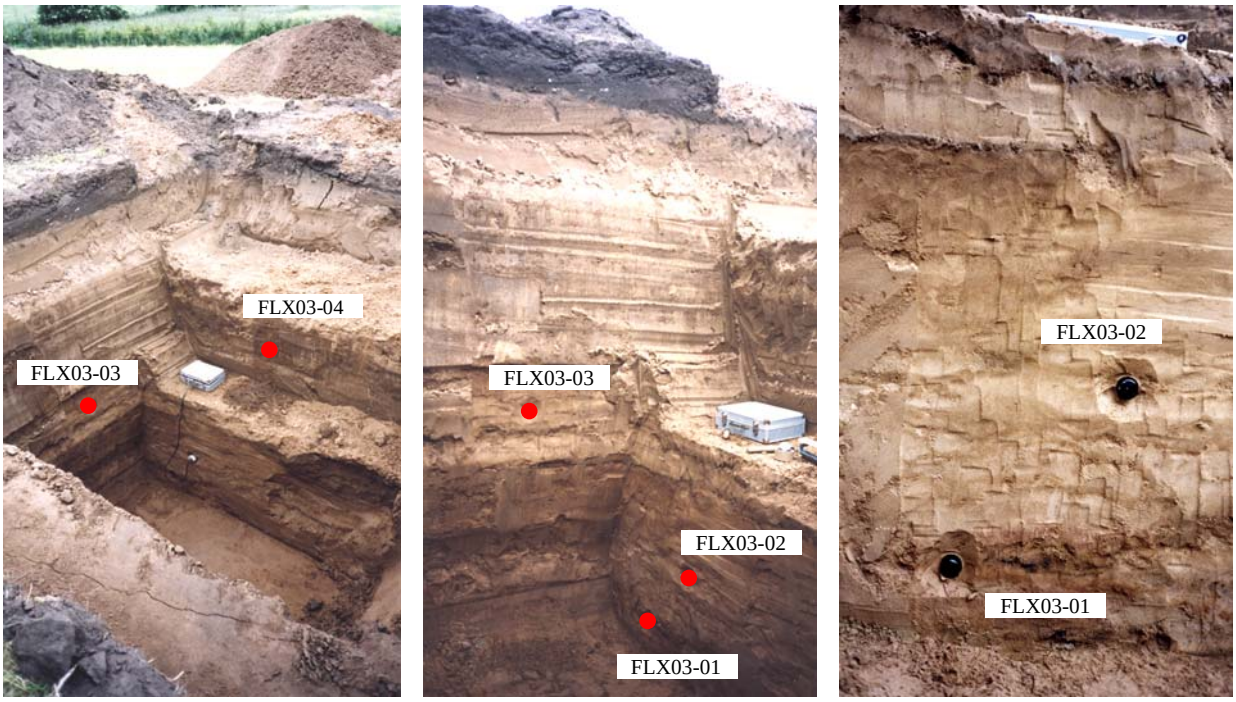

Figure 2 Location of OSL samples in Trench 3

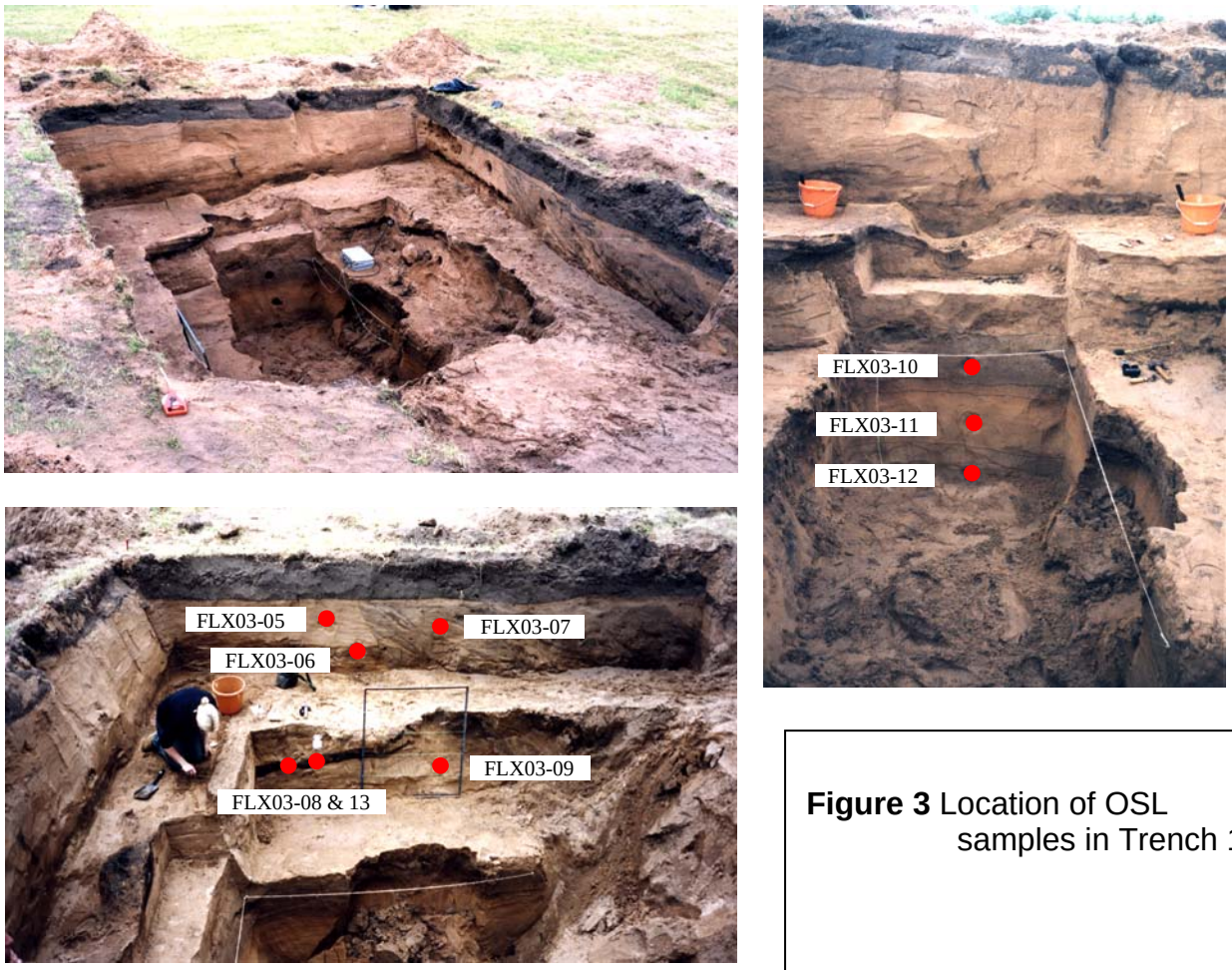

Figure 3 Location of OSL samples in Trench 1

Methods

The physical basis of luminescence dating

When ionising radiation (predominantly alpha, beta, or gamma radiation) interacts with an insulating crystal lattice (such as quartz or feldspar), a net redistribution of electronic charge takes place. Electrons are stripped from the outer shells of atoms and though most return immediately, a proportion escape and become trapped at meta-stable sites within the lattice. This charge redistribution continues for the duration of the radiation exposure and the amount of trapped charge is therefore related to both the duration and the intensity of radiation exposure. Even though trapped at meta-stable sites, electrons become 'free' if the crystal is subjected to heat or exposed to light. Once liberated, a free electron may become trapped once again or may return to a vacant position caused by the absence of a previously displaced electron (a 'hole'). This latter occurrence is termed 'recombination' and the location of the hole is described as the 'recombination centre'. As recombination occurs, a proportion of the energy of the electron is dissipated. Depending upon the nature of the centre where recombination occurs, this energy is expelled as heat and/or light. Therefore, when the crystal grain is either heated or illuminated following natural or artificial laboratory irradiation (the 'dose') the total amount of light emitted (luminescence) is directly related to the number of liberated electrons and available recombination sites. This is the fundamental principle upon which luminescence dating is based.

In cases where the duration of dosing is not known (as is the case for dating), estimates can be made from laboratory measurements. The response (the sensitivity) of the sample to radiation dose (ie the amount of light observed for a given amount of laboratory radiation, usually β-radiation) must be established. From this relationship the equivalent radiation exposure required to produce the same amount of light as that observed following the natural environmental dose can be determined, and is termed the palaeodose or 'equivalent dose' (D_e). The palaeodose (measured in Gy) is therefore an estimate of the total dose absorbed during the irradiation period. When the dose rate (the amount of radiation per unit time, measured in μGy/a) is measured (or calculated from measured concentrations of radionuclides), the duration of the dosing period can be calculated using the equation:

$$\text{Duration of dosing period} = \text{Palaeodose} \div \text{dose rate.}$$

The technique of optical dating was first applied to quartz by Huntley *et al* (1985), and methodological details were further developed by Smith *et al* (1986) and Rhodes (1988). The technique was demonstrated to work well for aeolian samples by Smith *et al* (1990), and has further proved to provide useful age estimates for a range of sedimentary contexts ranging from aeolian (eg Stokes *et al* 1997) to glacial contexts (Owen *et al* 1997). Further developmental research has introduced palaeodose measurement protocols that use a 'single aliquot regenerative-dose' (SAR) protocol (Murray and Wintle 2000). These protocols generally have the potential to provide improved accuracy (eg through correction of sensitivity change, interpolation rather than extrapolation of De values) as well as increased precision. In some cases they may also provide an indication of incomplete zeroing of the luminescence signal at the

time of deposition. Recent research within the laboratory (Rhodes *et al* 2003) has demonstrated the high precision and accuracy that may be achieved with this technique.

Sample preparation

The laboratory procedures were designed to yield pure quartz, of a particular grain size range, from the natural sediment samples. In order to obtain this material, samples were taken through a standard preparation procedure, as outlined below. All laboratory treatments were performed under low intensity laboratory safe-lighting, from purpose-built filtered sodium lamps (emitting at 588 nm).

After removal of the exposed ends of the sampling containers, the unexposed central portion of the sample was wet-sieved and the 180-255 µm grain size was used for dating (see Appendix 1 for details of specific samples). The chosen fraction was treated with hydrochloric acid (HCl) to remove carbonate and then treated in concentrated HF (48%) for 100 minutes. This treatment serves two purposes: (i) to dissolve feldspar grains, and (ii) to remove (etch) the outer surface of quartz grains (the only part of each quartz grain exposed during burial to natural alpha radiation). Any heavy minerals present were subsequently removed by gravity separation using a sodium polytungstate solution at 2.68 $g.cm^{-3}$. Finally, each sample was re-sieved to remove heavily etched grains. The order of the heavy liquid separation and second sieving are on occasion reversed for practical reasons, and for samples with extremely low yields, either or both of these treatments may be omitted after careful consideration. The prepared quartz samples were mounted on 1cm diameter aluminium discs for luminescence measurement using viscous silicone oil.

Various tests for sample purity are made. Sub-samples of the prepared material are examined using optical microscopy and the sample is exposed (within the Risø measurement system) to infrared (IR) light. Quartz generally does not produce measurable IR luminescence at room temperature whereas feldspar, which can suffer from anomalous fading of the infrared stimulated luminescence (IRSL) and OSL signals, or may be less rapidly bleached in some environments, produces an intense luminescence when stimulated with IR. The presence of a strong IRSL signal is therefore used as an indication for the presence of feldspar contaminants and is a criterion for rejection. In the rare cases where samples are rejected due to presence of high levels of IRSL, the prepared sediment sample is treated for ~ 2 weeks in concentrated H_2SiF_6 (silica-saturated HF), which effectively dissolves non-quartz material. If following this treatment, IRSL persists then the sample is subjected to a further two week H_2SiF_6 acid treatment before proceeding to the dating phase (luminescence measurement) and the results are interpreted with caution and the possible contamination of the sample discussed.

The measurement sequence adopted for dating all the samples included a post-IR blue OSL procedure (Banerjee *et al* 2001) designed to deplete any feldspar contribution to the OSL signal, by preceding each OSL measurement with an IRSL measurement. The IR exposure reduces the size of feldspar contributions, besides providing an alternative means to determine a palaeodose. For samples with strong

IRSL signals, significant feldspar contribution to the OSL may remain, and this is considered in the interpretation of the dates.

In order to determine the attenuating effect of pore water on the environmental dose rate of the sediments, additional samples were collected in the field and hermetically sealed. The moisture content of the sample was determined in the laboratory by weighing the sample before and after oven drying at 50°.

The single aliquot regenerative-dose (SAR) protocol

The SAR method is a regeneration procedure where the light level of the natural signal is converted into Gy via an interpolation between regenerated (ie known dose) points. The natural and regenerated signals are measured using the same aliquot. Sensitivity change commonly observed in quartz TL/OSL has previously precluded meaningful results being obtained this way. A key development reported by Murray and Wintle (2000) is that sample (aliquot) sensitivity is monitored following each OSL measurement (L_i) using the OSL response to a common test dose (S_i). Plots of L_i / S_i provide the necessary (sensitivity change corrected) data for interpolation. The procedure is further outlined in Figure 4.

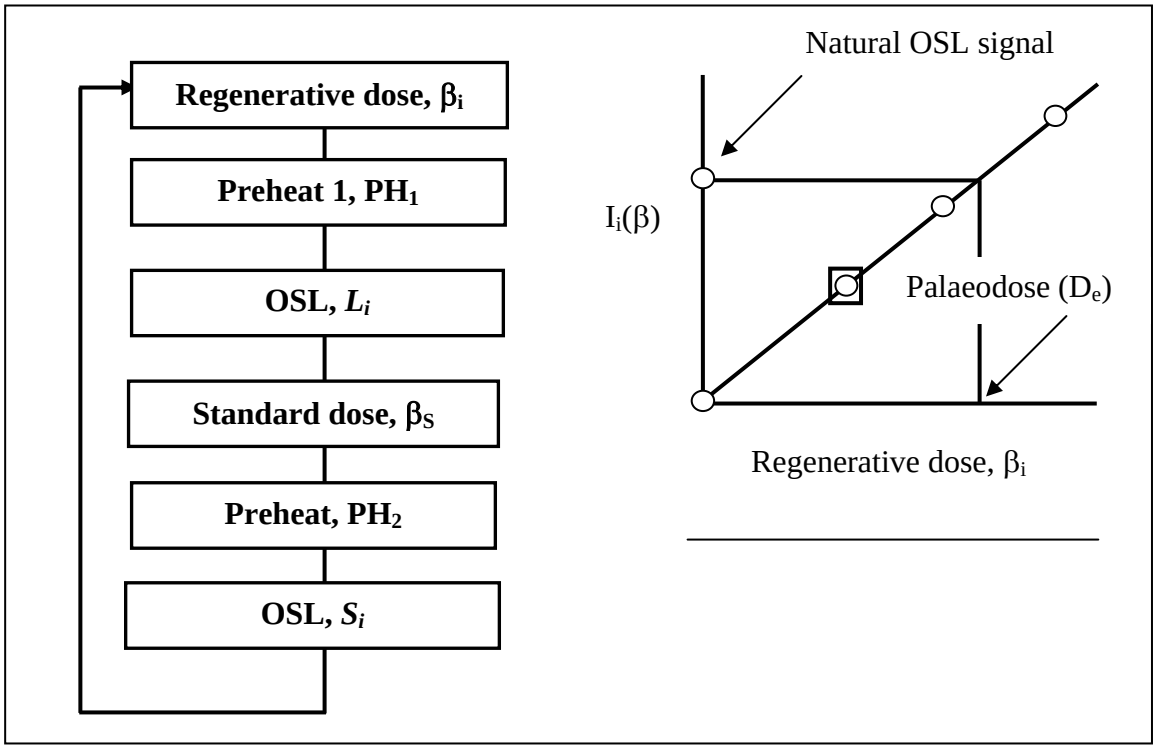

Figure 4 The SAR method. The procedure illustrated here is described in further detail in the text

Steps 1-6 are repeated n times in order to produce the data points required for interpolation (the first dose β_1 being zero, to give a measure of the natural signal). Typically n=7 (ie the natural plus 6 regeneration points, including one zero dose point and one repeat point). PH_1 and PH_2 are usually different although Murray and Wintle

(2000) report no dependence of the palaeodose on either (over the range of 200-280°C). The OSL signal is integrated over the initial part of the decay (to ~10% of initial intensity) and the background is taken as the light level measured at the end of each OSL measurement.

Murray and Wintle (2000) have introduced two further steps in to the measurement procedure. The first is the re-measurement of the first regenerated data point (indicated by the box in the explanatory Figure 2.1 above). The ratio of the two points (the "recycling ratio") provides an assessment of the efficacy of the sensitivity correction and the accuracy of the technique (large differences being suggestive of an ineffective technique). The recycling ratio (ideally unity) is typically in the range 0.95-1.05. The second additional step is a measurement of the regenerated OSL due to zero dose. This value gives a measure of the degree of thermal transfer to the trap(s) responsible for OSL during pre-heating. The ratio of this value to the natural OSL value (both corrected for sensitivity change) gives the "thermal transfer ratio" and ideally this should be in the range of 0.005-0.020.

Measurement procedures and conditions

Luminescence measurements were made using automated Risø luminescence measurement equipment. There are currently three different systems within the Luminescence Dating Laboratory that can be used for routine dating, the major difference between them being the optical stimulation sources. In two systems, optical excitation is provided by filtered blue diodes (emitting ~410-510nm), and in the third a filtered Halogen lamp (emitting ~420-560nm) is used. In all three systems, infrared stimulation is also provided using either an array of IR diodes or a single IR laser diode (depending on the measurement system). Luminescence is detected in the UV region on all systems, using EMI 9635Q bialkali photomultiplier tubes, filtered with Hoya U340 glass filters. Sample irradiation is provided in all cases by sealed ^{90}Sr sources at a rate of 1.5-3 Gy/minute depending on the system used.

The mean palaeodose for each sample was obtained from 12 aliquots (see Appendix 3 for further details regarding the statistics used in palaeodose and error calculations). All OSL measurements were made at 125°C (to ensure no re-trapping of charge to the 110°C TL trap during measurement) for between 50 and 100s, depending on the measurement system used. The signal detected in the initial first to second seconds (with the stable background count rate from the last 12 to 24 seconds subtracted) was corrected for sensitivity using the OSL signal regenerated by a subsequent beta dose (β_s). To ensure removal of unstable OSL components, removal of dose quenching effects, and to stimulate re-trapping and ensure meaningful comparison between naturally and laboratory irradiated signals, pre-heating was performed prior to each OSL measurement. Following each regenerative dose (β_i) and the natural dose, a pre-heat (PH_1) at 260°C for 10s was used for those samples with a palaeodose higher than 10 Gy (ie FLX03-01, FLX03-02, FLX03-11, and FLX03-12), whereas all the remaining samples were measured with a reduced pre-heat temperature set to 220°C. Following each test dose (β_s), a pre-heat (PH_2) of 220°C for 10s was applied to the older samples and in the case of the younger samples, this was reduced to 200°C for 10s (see Section 2.3 for further details of the SAR method). All the OSL

measurements incorporated a post-IR blue OSL stage in which each OSL measurement is preceded by an IRSL measurement at 50°C, to reduce the effects of any residual feldspar grains (Banerjee *et al* 2001) but the SAR procedure is otherwise unchanged.

For every sample, a routine internal laboratory procedure referred to as DELIA (D_e Luminescence Initial Assessment) was applied prior to the main SAR measurement in order to determine their approximate palaeodose value. This consisted in the use of a simplified version of the SAR measurement protocol applied to a limited number of three test discs in order to determine the internal variability, the OSL and TL signal form and sensitivity, as well as the magnitude of any IRSL signals. This considerably assists in the optimal selection of regenerative and test dose values, number of aliquots to measure, and the preheat combination selected. Quartz samples showing high levels of IRSL at this stage are given an extended (usually 14 days) treatment in fluorosilicic acid (H_2SiF_6). None of the samples from Flixborough required additional H_2SiF_6 treatment.

Results

The OSL dating results including age estimates, palaeodose, and environmental dose rate measurements are summarized in Table 2. Further details regarding individual samples may be found in Appendix 1. Factors affecting the dose rate determinations and the statistics used in error calculations are described in more detail in Appendices 2 and 3.

OSL age estimates are based on sand-sized quartz grains extracted from each sample and the measurement of 12 aliquots. Occasionally one or two discs were rejected from the calculation of the palaeodose. Dose rates were calculated by combining the results of neutron activation analysis (NAA) and *in situ* gamma-ray spectroscopy measurements. No or very low IRSL values above natural background were occasionally observed for some aliquots, suggesting good quartz separation had been achieved during sample preparation. Low palaedose variability between aliquots was observed in most samples and excellent agreement between one sample pair (X1691 & X1696).

All the samples displayed well defined luminescence signals and other OSL characteristics were also found to be well suited for SAR age determination. With the exception of sample X1695, all samples showed excellent recycling ratios, having mean sample recycling ratios less than 1% from unity. The size of the thermal transfer signal was found to be more variable, being generally below 5% but occasionally, as high as 15% for some aliquots. In the case of sample X1690, the thermal transfer was however found to be very variable and generally high (-2 to 200%). This sample was collected from a reworked near-surface sand deposit in trench 1 (see Fig 3) and was further characterized by relatively high inter-aliquot variation of the palaeodose values with a corresponding large error on the final age estimate. Although, a date was calculated for this sample the pattern of scatter in the palaeodose values strongly suggest incomplete zeroing (partial bleaching) of the OSL signal during a recent reworking event believed to be associated with a previous

excavation in the late 1990s. For this reason the date obtained for this sample should be interpreted with caution.

By contrast, the two replicate samples X1691 and X1696 collected from a black sand lens in trench 1 (see Fig 3) were found to possess exceptionally good signal characteristics with very rapid initial decays to a stable background level and typical of heat sensitised quartz. The improved signal sensitivity makes both these samples particularly well suited for OSL dating, manifesting as the lowest age uncertainties in this study (see Table 2). The measurements carried out on both replicate samples are also in excellent agreement with each other and provided very similar age estimates. Associated fragments of charcoal collected from the same sedimentary unit could provide good independent assessment of the performance of OSL dating if samples can be submitted for radiocarbon dating in the future.

Overall, the observed luminescence characteristics (good sensitivity, low variability, good recycling, and relatively low thermal transfer values) strongly suggest that the calculated age estimates are reliable. The luminescence dating results appear to be broadly consistent with the archaeological expectations, suggesting that the measured OSL signals were sufficiently stable, and with the exception of sample X1690, had undergone complete zeroing at the time of deposition.

The age estimates obtained from samples in both trenches are generally in good stratigraphic order, but the basal sample X1684 in trench 3 displays an apparent age inversion with respect to the overlying sample X1685. Although the errors of both samples just about overlap, it seems that the age estimate for X1684 may be slightly underestimated. A possible explanation for this may be due to a small increase in the concentrations of radioactive elements at this sampling depth. This could be due to post-depositional translocation of fine mineral particles from the weathering of the overlying sand deposits or alternatively, the lateral influx and concentration of material with the movement of groundwater. The gradual accumulation of silt size debris in the basal sediments may explain the higher environmental dose rate measured at this sampling location (see Table 2 and Appendix 1). The overestimate of the true average dose rate could explain the apparent age underestimate. If the age is recalculated using the average concentrations of potassium, thorium, and uranium as determined by the NAA results from the overlying sediments then the age of sample X1684 is 10750±1070 years BP. This would appear to be in better agreement with the estimate of 11190±1360 years BP obtained for the overlying sample.

Field code	**Lab. code**	**Trench**	**Palaeodose** (Gy)	**Dose rate** (mGy/a)	**Age estimate code**	**OSL date** (years before 2003) ± 1 sigma
FLX03-01	X1684	Trench 3	15.52 ± 1.24	1.70 ± 0.09	OxL-1477	9110 ± 880
FLX03-02	X1685	Trench 3	16.21 ± 1.76	1.45 ± 0.07	OxL-1478	11190 ± 1360
FLX03-03	X1686	Trench 3	3.29 ± 0.12	1.53 ± 0.08	OxL-1479	2150 ± 150
FLX03-04	X1687	Trench 3	1.84 ± 0.13	1.44 ± 0.08	OxL-1480	1280 ± 120
FLX03-05	X1688	Trench 1	3.34 ± 0.18	1.48 ± 0.09	OxL-1481	2260 ± 190
FLX03-06	X1689	Trench 1	2.95 ± 0.15	1.54 ± 0.09	OxL-1482	1920 ± 160
FLX03-07	X1690	Trench 1	0.68 ± 0.40	1.58 ± 0.10	OxL-1483	430 ± 250
FLX03-08	X1691	Trench 1	2.95 ± 0.08	1.27 ± 0.06	OxL-1484	2320 ± 140
FLX03-09	X1692	Trench 1	2.52 ± 0.06	1.45 ± 0.09	OxL-1485	1740 ± 120
FLX03-10	X1693	Trench 1	4.61 ± 0.16	1.49 ± 0.08	OxL-1486	3080 ± 210
FLX03-11	X1694	Trench 1	17.51 ± 1.19	1.55 ± 0.09	OxL-1487	11030 ± 1010
FLX03-12	X1695	Trench 1	19.20 ± 0.79	1.82 ± 0.09	OxL-1488	10570 ± 720
FLX03-13	X1696	Trench 1	3.10 ± 0.09	1.27 ± 0.07	OxL-1489	2430 ± 150

Table 2 Summary of OSL dating results. The results are based on luminescence measurements of sand-sized quartz (180-255μm). All samples were measured using a SAR post-IR blue OSL protocol (Murray and Wintle 2000; Banerjee *et al* 2001). Gamma dose rates are based on *in situ* gamma-ray spectroscopy measurements. Beta dose rate values were calculated using the concentrations of uranium, thorium, and potassium as determined by neutron activation analysis (NAA). Corrections were made in the age calculation for the water content of the sediment samples using the correction factors outlined in Aitken (1985) and taken from Zimmermann (1971). The contribution of cosmic radiation was calculated as a function of latitude, altitude, burial depth and average over-burden density according to the formulae of Prescott and Hutton (1994). Further details regarding individual samples may be found in Appendix 1

A similar situation is observed for the basal sediments in trench 1, although here the effect is less noticeable. Sample X1695 is slightly younger than the overlying sample X1694 but the OSL age estimates and their overlapping respective errors are sufficiently close and the differences do not require any special considerations. The only problematic issue relates to sample X1692 which provided an age estimate (see Table 3.1) considerably younger than that obtained from the overlying pair of samples (X1691 and X1696). The latter were mentioned earlier in the discussion as

possessing ideal OSL characteristics and hence are believed to provide the more reliable age estimates. The NAA results obtained for sample X1692 (see Appendix 1) show that this was the only sample for which the concentration of uranium was below the detection limit (less than 0.5ppm). A value of 0.2 ppm with a relatively large error of 0.1 ppm was used for the age calculation and this value is unlikely to have been much lower than this approximation. A possible explanation may be due to the small but persistent IRSL signal recorded for aliquots from this sample. Because most aliquots were affected by this potential source of feldspar contamination it was not possible to derive a statistically meaningful age estimate by eliminating some of the aliquots from the palaeodose calculation. This sample could benefit from additional 2-4 weeks treatment in fluorosilicic acid to dissolve feldspar minerals prior to re-measurement of the OSL signal. In the meantime, the age estimate provided here should be interpreted with caution.

Conclusion

The observed luminescence characteristics (good sensitivity, good recycling ratios, and relatively low thermal transfer values) combined with a low degree of scatter in the palaeodose distributions, strongly suggest that the calculated palaeodose values are accurate and precise. Optical dates based on the measurement of the optically stimulated luminescence (OSL) signal from quartz indicate two clear phases of aeolian activity in the early and late Holocene, separated by a long period of relative landscape stability. The dates within individual stratigraphic units show close agreement and allow the chronology of dune and sand sheet reactivation events to be accurately reconstructed. The OSL dating results appear to be broadly consistent with the archaeological expectations, suggesting that the measured signals were sufficiently stable, and with the exception of sample X1690, had undergone complete zeroing at the time of deposition.

The OSL dating programme carried out as part of the Lincolnshire coversand project suggests that in optimal circumstances, luminescence dating may be able to provide resolution at 1 standard deviation approaching 6%. The technique may therefore be capable of delivering high resolution site chronologies similar to those based on calibrated radiocarbon dates.

OSL dating clearly has potential for dating sediment accumulation and reworking in the coversand landscape of North Lincolnshire and for providing a *terminus post quem* or *ante quem* for phases of human activity and buried structures. In these sandy regions, the aeolian depositional environment is likely to have favoured sufficient exposure to daylight during transport to enable complete resetting of the OSL signal prior to deposition. Optical dating thus enables assessment of the rate and timing of periods of sand accumulation at archaeological sites. Dating series of samples as opposed to only a few isolated single samples, provides both an assessment of the degree of coherence provided by the technique (by assessing the degree of age inversion in the sample column), and information about sand accumulation and periods of relative environmental quiescence. Sandy deposits which are generally unfavourable to the preservation of organic material and hence, offer limited material suitable for radiocarbon dating, are by contrast well suited for OSL dating.

References

Aitken, M J, 1985 *Thermoluminescence dating,* London (Academic Press)

Banerjee, D, Murray, A S, Bøtter-Jensen, L, and Lang, A, 2001 Equivalent dose estimation using a single aliquot of polymineral fine grains, *Radiation Measurements*, **33**, 73-94

Bateman, M D, 1995 Thermoluminescence dating of the British coversand deposits, *Quat Sci Rev,* **14**, 791-8

Bateman, M D, 1998 The origin and age of coversand in north Lincolnshire, UK, *Permafrost and Periglacial Processes*, **9**, 313–25

Bateman, M D, Murton, J B, and Crowe, W, 2000 Reconstruction of the depositional environments associated with the Late Devensian and Holocene coversand around Caistor, north Lincolnshire, UK, *Boreas*, **29**, 1-16

Huntley, D J, Godfrey-Smith, D I, and Thewalt, M L W, 1985 Optical dating of sediments, *Nature*, **313**, 105-7

Mejdahl, V, 1979 Thermoluminescence dating: beta dose attenuation in quartz grains, *Archaeometry*, **21**, 61-73

Murray, A S, and Wintle, A G, 2000 Luminescence dating of quartz using an improved single-aliquot regenerative-dose protocol, *Radiation Measurements,* **32**, 57-73

Owen, L A, Mitchell, W A, Bailey, R M, Coxon, P, and Rhodes, E J, 1997 Style and timing of glaciation in the Lahul Himalaya, northern India: a frame work for reconstructing Late Quaternary palaeoclimatic change in the western Himalayas, *J Quat Sci*, **12**, 83-109

Prescott, J R, and Hutton, J T, 1994 Cosmic ray contributions to dose rates for luminescence and ESR dating: large depths and long term time variations, *Radiation Measurements,* **23**, 497-500

Rhodes, E J, 1988 Methodological considerations in the optical dating of quartz, *Quat Sci Rev*, **7**, 395-400

Rhodes, E J, Bronk-Ramsey, C, Outram, Z, Batt, C, Willis, L, Dockrill, S, Batt, C, and Bond, J, 2003 Bayesian methods applied to the interpretation of multiple OSL dates: high precision sediment age estimates from Old Scatness Broch excavations, Shetland Isles, *Quat Sci Rev*, **22**, 1231-44

Smith, B W, Aitken, M J, Rhodes, E J, Robinson, P D, and Geldard, D M, 1986 Optical dating: methodological aspects, *Radiation Protection Dosimetry,* **17**, 229-33

Smith, B W, Rhodes, E J, Stokes, S, Spooner, N A, and Aitken, M J, 1990 Optical dating of sediments: initial results from Oxford, *Archaeometry*, **32**, 19-31

Stokes, S, Thomas, D S G, and Washington R W, 1997 Multiple episodes of aridity in southern Africa since the last interglacial period, *Nature,* **388**, 154-9

Zimmermann, D.W. 1971 Thermoluminescent dating using fine grains from pottery, *Archaeometry*, **13**, 29-52

Appendix 1: Details of radioactivity data and age calculations

Field code Laboratory code	FLX03-01 X1684	FLX03-02 X1685	FLX03-03 X1686	FLX03-04 X1687	FLX03-05 X1688	FLX03-06 X1689	FLX03-07 X1690
Palaeodose (Gy)	15.52	16.21	3.29	1.84	3.34	2.95	0.68
uncertainty	1.28	1.79	0.14	0.14	0.19	0.16	0.40
measured	1.24	1.76	0.12	0.13	0.18	0.15	0.40
Grain size							
Min. grain size (µm)	180	180	180	180	180	180	180
Max grain size (µm)	255	255	255	255	255	255	255
External gamma-dose (Gy/ka)	0.641	0.560	0.516	0.487	0.435	0.436	0.453
error	0.002	0.002	0.002	0.001	0.001	0.002	0.001
Measured concentrations							
standard fractional error	0.050	0.050	0.050	0.050	0.050	0.050	0.050
% K	1.180	1.020	1.180	1.080	1.050	1.160	1.200
error (%K)	0.059	0.051	0.059	0.054	0.053	0.058	0.060
Th (ppm)	4.790	2.580	3.400	3.870	2.440	2.930	2.740
error (ppm)	0.240	0.129	0.170	0.194	0.122	0.147	0.137
U (ppm)	1.190	0.550	0.910	0.570	0.610	0.590	0.600
error (ppm)	0.060	0.028	0.046	0.029	0.031	0.030	0.030
Cosmic dose calculations							
Depth (m)	3.750	3.350	2.500	2.000	0.650	1.000	0.650
error (m)	0.100	0.100	0.100	0.100	0.100	0.100	0.100
Average overburden density (g.cm^3)	1.900	1.900	1.900	1.900	1.900	1.900	1.900
error (g.cm^3)	0.100	0.100	0.100	0.100	0.100	0.100	0.100
Latitude (deg.), north positive	53	53	53	53	53	53	53
Longditude (deg.), east positive	0	0	0	0	0	0	0
Altitude (m above sea-level))	20	20	20	20	20	20	20
Cosmic dose rate (µGy/ka)	0.131	0.137	0.152	0.162	0.193	0.185	0.193
error	0.010	0.011	0.013	0.014	0.033	0.023	0.033
Moisture content							
Moisture (water / wet sediment)	0.128	0.104	0.138	0.128	0.034	0.046	0.052
error	0.050	0.050	0.050	0.050	0.050	0.050	0.050
Total dose rate, Gy/ka	**1.70**	**1.45**	**1.53**	**1.44**	**1.48**	**1.54**	**1.58**
error	**0.09**	**0.07**	**0.08**	**0.08**	**0.09**	**0.09**	**0.10**
% error	**5.03**	**5.06**	**5.37**	**5.31**	**6.01**	**6.00**	**6.14**
AGE (ka)	**9.11**	**11.19**	**2.15**	**1.28**	**2.26**	**1.92**	**0.43**
error	**0.88**	**1.36**	**0.15**	**0.12**	**0.19**	**0.16**	**0.25**
% error	**9.65**	**12.15**	**6.79**	**9.19**	**8.32**	**8.11**	**59.18**

Appendix 1: continued

Field code Laboratory code	FLX03-01 X1684	FLX03-02 X1685	FLX03-03 X1686	FLX03-04 X1687	FLX03-05 X1688	FLX03-06 X1689	FLX03-07 X1690
Average beta-attenuation							
standard fractional error	0.050	0.050	0.050	0.050	0.050	0.050	0.050
Natural U	0.846	0.846	0.846	0.846	0.846	0.846	0.846
error	0.042	0.042	0.042	0.042	0.042	0.042	0.042
Th-232	0.787	0.787	0.787	0.787	0.787	0.787	0.787
error	0.039	0.039	0.039	0.039	0.039	0.039	0.039
K-40	0.924	0.924	0.924	0.924	0.924	0.924	0.924
error	0.046	0.046	0.046	0.046	0.046	0.046	0.046
Dose rate conversion (Gy/ka)							
standard fractional error	0.050	0.050	0.050	0.050	0.050	0.050	0.050
U (ppm)							
Beta	0.146	0.146	0.146	0.146	0.146	0.146	0.146
error	0.007	0.007	0.007	0.007	0.007	0.007	0.007
Gamma	0.000	0.000	0.000	0.000	0.000	0.000	0.000
error	0.000	0.000	0.000	0.000	0.000	0.000	0.000
Th (ppm)							
Beta	0.027	0.027	0.027	0.027	0.027	0.027	0.027
error	0.001	0.001	0.001	0.001	0.001	0.001	0.001
Gamma	0.000	0.000	0.000	0.000	0.000	0.000	0.000
error	0.000	0.000	0.000	0.000	0.000	0.000	0.000
K (%)							
Beta	0.782	0.782	0.782	0.782	0.782	0.782	0.782
error	0.039	0.039	0.039	0.039	0.039	0.039	0.039
Gamma	0.000	0.000	0.000	0.000	0.000	0.000	0.000
error	0.000	0.000	0.000	0.000	0.000	0.000	0.000
Cosmic dose							
Geomagnetic latitude	55.7	55.7	55.7	55.7	55.7	55.7	55.7
Dc (Gy/ka), 55N G.lat, 0 km Alt.	0.130	0.136	0.152	0.161	0.193	0.184	0.193
error	0.010	0.011	0.013	0.014	0.033	0.023	0.033
Moisture							
F	0.383	0.341	0.400	0.383	0.188	0.220	0.234
error	0.106	0.116	0.103	0.106	0.195	0.169	0.159
W	0.383	0.341	0.400	0.383	0.188	0.220	0.234
error	0.106	0.116	0.103	0.106	0.195	0.169	0.159
WF	0.147	0.116	0.160	0.147	0.035	0.048	0.055
error	0.057	0.056	0.058	0.057	0.052	0.052	0.053
Age uncertainties	1.000	1.000	1.000	1.000	1.000	1.000	1.000
dDR/K	0.610	0.631	0.602	0.610	0.692	0.681	0.676
dDR/dC(B, K)	0.921	0.823	0.908	0.843	0.929	1.010	1.037
dDR/dA(K)	0.780	0.697	0.769	0.714	0.786	0.856	0.878
dDR/dTh	0.018	0.019	0.018	0.018	0.021	0.020	0.020
dDR/dC(B, Th)	3.184	1.772	2.229	2.572	1.839	2.174	2.017
dDR/dA(Th)	0.110	0.062	0.077	0.089	0.064	0.075	0.070
dDR/dU	0.104	0.108	0.103	0.104	0.118	0.117	0.116
dDR/dC(B, U)	0.715	0.739	0.705	0.715	0.811	0.798	0.792
dDR/dA(U)	0.147	0.070	0.111	0.070	0.085	0.081	0.082
dDR/dW	-0.377	-0.279	-0.360	-0.319	-0.191	-0.238	-0.256
dDR/dF	-0.377	-0.279	-0.360	-0.319	-0.191	-0.238	-0.256
dDR/C(G, K)	1.011	0.901	0.998	0.925	1.009	1.100	1.129
dDR/C(G, Th)	4.103	2.279	2.875	3.315	2.346	2.777	2.579
dDR/dC(G, U)	1.019	0.486	0.770	0.488	0.586	0.559	0.565
dDR/dCosmic	1.000	1.000	1.000	1.000	1.000	1.000	1.000
Dage/dDe	0.587	0.690	0.652	0.695	0.677	0.650	0.632
Dage/dDR	-5.350	-7.728	-1.400	-0.890	-1.531	-1.246	-0.272

Appendix 1: continued

Field code Laboratory code	FLX03-08 X1691	FLX03-09 X1692	FLX03-10 X1693	FLX03-11 X1694	FLX03-12 X1695	FLX03-13 X1696
Palaeodose (Gy)	2.95	2.52	4.61	17.51	19.20	3.10
uncertainty	0.10	0.08	0.18	1.24	0.88	0.11
measured	0.08	0.06	0.16	1.19	0.79	0.09
Grain size						
Min. grain size (µm)	180	180	180	180	180	180
Max grain size (µm)	255	255	255	255	255	255
External gamma-dose (Gy/ka)	0.439	0.401	0.463	0.526	0.638	0.439
error	0.002	0.002	0.002	0.002	0.002	0.002
Measured concentrations						
standard fractional error	0.050	0.050	0.050	0.050	0.050	0.050
% K	1.000	1.190	1.150	1.140	1.250	1.010
error (%K)	0.050	0.060	0.058	0.057	0.063	0.051
Th (ppm)	2.690	2.080	3.100	2.610	7.670	2.470
error (ppm)	0.135	0.104	0.155	0.131	0.384	0.124
U (ppm)	0.680	<0.500	0.940	0.680	1.490	0.510
error (ppm)	0.034	0.100	0.047	0.034	0.075	0.026
Cosmic dose calculations						
Depth (m)	1.450	1.600	2.100	2.500	3.000	1.500
error (m)	0.100	0.100	0.100	0.100	0.100	0.100
Average overburden density (g.cm^3)	1.900	1.900	1.900	1.900	1.900	1.900
error (g.cm^3)	0.100	0.100	0.100	0.100	0.100	0.100
Latitude (deg.), north positive	53	53	53	53	53	53
Longditude (deg.), east positive	0	0	0	0	0	0
Altitude (m above sea-level))	20	20	20	20	20	20
Cosmic dose rate (µGy/ka)	0.174	0.171	0.160	0.152	0.143	0.173
error	0.017	0.016	0.014	0.013	0.011	0.017
Moisture content						
Moisture (water / wet sediment)	0.199	0.046	0.115	0.078	0.143	0.181
error	0.050	0.050	0.050	0.050	0.050	0.050
Total dose rate, Gy/ka	**1.27**	**1.45**	**1.49**	**1.55**	**1.82**	**1.27**
error	**0.06**	**0.09**	**0.08**	**0.09**	**0.09**	**0.07**
% error	**5.08**	**6.30**	**5.57**	**5.50**	**5.08**	**5.18**
AGE (ka)	**2.32**	**1.74**	**3.08**	**11.30**	**10.57**	**2.43**
error	**0.14**	**0.12**	**0.21**	**1.01**	**0.72**	**0.15**
% error	**6.14**	**7.03**	**6.86**	**8.97**	**6.83**	**6.27**

Appendix 1: continued

Field code Laboratory code	FLX03-08 X1691	FLX03-09 X1692	FLX03-10 X1693	FLX03-11 X1694	FLX03-12 X1695	FLX03-13 X1696
Average beta-attenuation						
standard fractional error	0.050	0.050	0.050	0.050	0.050	0.050
Natural U	0.846	0.846	0.846	0.846	0.846	0.846
error	0.042	0.042	0.042	0.042	0.042	0.042
Th-232	0.787	0.787	0.787	0.787	0.787	0.787
error	0.039	0.039	0.039	0.039	0.039	0.039
K-40	0.924	0.924	0.924	0.924	0.924	0.924
error	0.046	0.046	0.046	0.046	0.046	0.046
Dose rate conversion (Gy/ka)						
standard fractional error	0.050	0.050	0.050	0.050	0.050	0.050
U (ppm)						
Beta	0.146	0.146	0.146	0.146	0.146	0.146
error	0.007	0.007	0.007	0.007	0.007	0.007
Gamma	0.000	0.000	0.000	0.000	0.000	0.000
error	0.000	0.000	0.000	0.000	0.000	0.000
Th (ppm)						
Beta	0.027	0.027	0.027	0.027	0.027	0.027
error	0.001	0.001	0.001	0.001	0.001	0.001
Gamma	0.000	0.000	0.000	0.000	0.000	0.000
error	0.000	0.000	0.000	0.000	0.000	0.000
K (%)						
Beta	0.782	0.782	0.782	0.782	0.782	0.782
error	0.039	0.039	0.039	0.039	0.039	0.039
Gamma	0.000	0.000	0.000	0.000	0.000	0.000
error	0.000	0.000	0.000	0.000	0.000	0.000
Cosmic dose						
Geomagnetic latitude	55.7	55.7	55.7	55.7	55.7	55.7
Dc (Gy/ka), 55N G.lat, 0 km Alt.	0.173	0.170	0.159	0.152	0.142	0.172
error	0.017	0.016	0.014	0.013	0.011	0.017
Moisture						
F	0.498	0.220	0.360	0.291	0.408	0.470
error	0.089	0.169	0.111	0.132	0.101	0.092
W	0.498	0.220	0.360	0.291	0.408	0.470
error	0.089	0.169	0.111	0.132	0.101	0.092
WF	0.248	0.048	0.130	0.085	0.167	0.221
error	0.062	0.052	0.056	0.054	0.058	0.061
Age uncertainties	1.000	1.000	1.000	1.000	1.000	1.000
dDR/K	0.551	0.681	0.621	0.653	0.598	0.566
dDR/dC(B, K)	0.705	1.037	0.914	0.952	0.955	0.731
dDR/dA(K)	0.597	0.878	0.774	0.806	0.809	0.619
dDR/dTh	0.016	0.020	0.018	0.019	0.018	0.017
dDR/dC(B, Th)	1.615	1.543	2.098	1.857	4.992	1.522
dDR/dA(Th)	0.056	0.054	0.073	0.064	0.173	0.053
dDR/dU	0.094	0.117	0.106	0.112	0.102	0.097
dDR/dC(B, U)	0.646	0.798	0.728	0.765	0.700	0.663
dDR/dA(U)	0.076	0.028	0.118	0.090	0.180	0.058
dDR/dW	-0.313	-0.227	-0.338	-0.286	-0.438	-0.305
dDR/dF	-0.313	-0.227	-0.338	-0.286	-0.438	-0.305
dDR/C(G, K)	0.779	1.128	1.002	1.040	1.050	0.807
dDR/C(G, Th)	2.096	1.972	2.700	2.380	6.444	1.973
dDR/dC(G, U)	0.530	0.190	0.819	0.620	1.252	0.407
dDR/dCosmic	1.000	1.000	1.000	1.000	1.000	1.000
Dage/dDe	0.786	0.691	0.669	0.645	0.550	0.785
Dage/dDR	-1.824	-1.203	-2.064	-7.295	-5.817	-1.909

Appendix 2: Dose rate determination

Radiation dose is measured in energy units of Gray (Gy), the standard SI unit of absorbed dose (1 Gy = 1 Joule/kg). The measurement of dose rate (or annual dose) can be made using a variety of different methods. For most samples, the majority of the environmental dose rate is due to the radioactive decay of unstable isotopes of potassium (K), uranium (U) and daughter isotopes, and thorium (Th) and daughter isotopes. A further small fraction comes from the cosmic dose rate, and is a function of altitude, geomagnetic latitude, and overburden thickness and density (Prescott and Hutton 1994). Water content attenuates the environmental dose rate, and uncertainties in the average of this value over the burial period may often form a significant contribution to the overall uncertainty in the age estimate.

In situ gamma spectrometry

Portable gamma spectrometer readings may be taken at each sampling location. The probe (housing an NaI scintillator crystal) is inserted into a deepened hole excavated following the retrieval of the OSL sample. Measurements typically take up to one hour and result in the direct estimation of the total *in situ* gamma radiation field. The spectra are also used to estimate contributions from U, Th, and K individually. Through comparison to known concentration standards, quantitative estimates of U, Th, and K concentrations are made.

Neutron Activation Analysis

A representative sub-sample (typically 10-20g, though as little as 80mg may be used with specialised procedures) of the sample is sent for commercial analysis. The analysis involves an initial (neutron) irradiation of each sample. This causes the creation of many new short-lived isotopes whose concentration depend on the bulk chemical composition of the original sample. This leaves the samples in a highly unstable (ie radioactive) state. The different gamma emissions from the radioactive decay of the sample are then measured using high resolution gamma-spectrometry. These measurements yield estimates of U, Th, and K concentration. The measurement of K and Th are usually precise, though samples with low levels of U may be below the detection limit for this element, depending on the interferences from other isotopes. The direct measurement of a small volume renders this method very well suited for the estimation of beta dose rate.

Moisture content of the sample

Moisture within the pore spaces of sediments absorbs α, β, and γ-radiation. As a result, less is absorbed by the mineral grains. It is therefore important to assess the present day water content of the sediment and to make some assessment of the variability of moisture throughout the burial period of the sample. The moisture correction factors outlined in Aitken (1985) and taken from Zimmermann (1971) are used in the age calculation (Appendix 1).

Cosmic dose rate

The contribution of cosmic radiation to the total dose rate is calculated as a function of (geomagnetic) latitude, altitude, burial depth, and average over-burden density, according to the formulae of Prescott and Hutton (1994).

Radiation attenuation factors

For coarse grains, the portion of the sample that receives an α-dose is removed by HF etching. Therefore, no consideration of the α-dose is made during the age calculation. β-particles (electrons) are significantly attenuated (ie a large fraction of the energy is absorbed) as the β-particle passes through a grain. Account of this effect is needed in order to correctly estimate the dose received by the 'average' grain. The so-called 'attenuation factors' are taken from the empirical work of Mejdahl (1979).

The γ-dose is assumed to be unaffected by attenuation as the penetration of gamma-rays through sediments is several orders of magnitude greater than (~10^5 times) the size of individual grains. Consequently, no attenuation factors are applied to the γ-dose.

Results for the U, Th (ppm), and K (%) concentration of each sample, together with the other parameters used in the age calculation, are provided in Appendix 1.

Appendix 3: Statistics and error calculation

The calculated age depends on the estimate of total absorbed dose (D_e) and the dose rate (D_R). Both of these estimates have uncertainties associated with them. This appendix gives general details of how the 'error' (the statistical uncertainty) is calculated for each term and combined with the errors on other terms to give an overall estimate of uncertainty on the OSL age estimate.

Palaeodose estimation

As described in a previous section (Figure 2.1), individual estimates of palaeodose also referred to as D_e are obtained from each of the aliquots (sub-samples) measured, using the SAR technique. The value of the D_e is obtained by interpolating between the points of the dose response curve. Statistical uncertainties are calculated for each of the individual points and also on the interpolated value of D_e. Typically, 12 aliquots are measured for each sample.

Each of the points on the growth curve is defined as:

$$I(\beta)_i = \frac{L_i - f \cdot l_i}{S_i - f \cdot s_i \cdot} \qquad \text{Equation 1}$$

where L_i is the integrated (initial) OSL from the regeneration dose and l_i is the measured background signal, S_i is the integrated (initial) OSL from the test dose (see Section 3) and s_i is the background; f is a scaling factor included to take account of the difference in duration of the L_i,S_i, and l_i,s_i measurements.

The error on each dose-response data point (see Figure 2.1) is calculated by propagating 'counting statistics' errors (assuming Poisson statistics) from the integration of raw OSL data. The error on each term in Equation 1 is given by the square-root of the value. For example, the range for L_i is given by $L_i \pm \sqrt{L_i}$. The errors on each value are propagated in the standard way (see below) to give the uncertainty of $I(\beta)_i$.

In cases where the dose response can be (locally) approximated by a straight line, a weighted least squares linear fit is used. The errors in this case are calculated analytically using standard formulae.

In cases where the dose response is significantly non-linear, a single saturating exponential function is used to describe the dose response (a Simplex algorithm is used for fitting in this case). Occasionally an extra linear term is added to the exponential term in order to better describe the form of the dose response, although this is not commonly necessary. The uncertainty for non-linear fitting is calculated using a Monte-Carlo method in which 'random samples' of the dose response data are taken (assuming normally distributed probabilities) and used to obtain the

palaeodose value. The spread in these values is then used to calculate the error on the mean palaeodose for each aliquot, giving a range for each palaeodose of $D_{ei} \pm \sigma D_{ei}$

Once the individual D_e values have been obtained from each aliquot (and the associated uncertainties calculated) the values are grouped to give a final overall estimate of D_e. The final D_e estimate is calculated using a weighted average. The weight of each D_e is referred to as w_i and defined as:

$$w_i = \frac{1}{\sigma D_{ei}^2} \Big/ \sum_i \frac{1}{\sigma D_{ei}^2} \qquad \text{Equation 2}$$

The weighted mean is defined as:

$$\overline{D}_e = \sum_i D_{ei} \cdot w_i \qquad \text{Equation 3}$$

The weighted standard error, $\hat{\sigma}_{\overline{x}w}$, is calculated from:

$$\hat{\sigma}_{\overline{x}w} = \sqrt{\frac{\sum_i w_i \left(D_{ei} - \overline{D}_e\right)}{1 - \frac{1}{n}}} \Big/ \sqrt{n} \qquad \text{Equation 4}$$

where n is the number of aliquots. The range of the weighted mean D_e is then defined as:

$$\overline{D}_e \pm \hat{\sigma}_{\overline{x}w} \qquad \text{Equation 5}$$

Slight modifications to the approach outlined above are made in special circumstances, though in most cases this description is sufficient.

Dose rate

The errors on the dose rate are due to errors in a range of values, for example, the concentration of U, Th, and K, as well as the water content of the sample. The individual components of the dose rate calculation are shown in Appendix 1. The uncertainty on the overall dose rate is calculated by combining the uncertainties according to the standard propagation formula given below.

Age calculation

The calculated age is obtained from dividing the mean palaeodose (Equation 3) by the total dose rate (Appendix 1). The uncertainty on the final age estimate is calculated using the error propagation formula given below. All calculations were performed using software developed within the laboratory.

Standard error propagation

If a calculated value (y) is calculated using a function (f) which contains terms x_1, x_2, x_3.... x_n , then,

$$y = f(x_1, x_2, x_3 ... x_n) \qquad \text{Equation 6}$$

Each term (x_i) has an associated uncertainty with a range expressed as $x_i \pm \sigma_{xi}$. The overall error of y can be calculated through the addition of the partial derivatives of y with respect to each term. Formally, this is written as:

$$\sigma_y = \sqrt{\sum_i \left(\frac{\partial y}{\partial x_i} \cdot \sigma_{xi} \right)^2} \qquad \text{Equation 7}$$

giving a range for y as $y \pm \sigma_Y$.